Low-noise Wideband Circuit for Closed-loop RF CNT-NEMS Sensors

Christian Kauth, Marc Pastre, and Maher Kayal

***Abstract*—Hybrid NEMS interfaces are the key to systems combining the benefits of highly sensitive miniaturized mechanical sensors with the vast functionalities available in electronics. In this context, a phase-locked loop, locking on a suspended resonating carbon nanotube NEMS, is implemented and characterized, able to start, track, amplify and sustain NEMS oscillation up to 100MHz in a sensing environment. Detection of the signals out of the NEMS has been found most challenging and diverse RF front-ends meant for interfacing high-impedance carbon nanotube based NEMS are analyzed. Given the feeble signals from the NEMS, their high output impedance and non-negligible interconnect parasitics, front-end design must imperatively focus on minimal noise figure. Limits on minimal detectable signal are extracted via design, simulation and characterization of a 3-stage common-emitter front-end.**

***Index Terms*—Signal to noise ratio, Signal detection, Noise figure, Low-noise amplifiers, Wideband, Piezoresistance, Nanoelectromechanical systems, Oscillators.**

I. Introduction

CARBON nanotube nanoelectromechanical systems (CNT-NEMS) start finding their way to sensor applications. Their small dimensions and high resonance frequencies make them candidates for high-resolution sensing of physical and chemical phenomena [1]. Electronic detection of the mechanical resonance plays a crucial role in the sensing process. So far, most experiments relied on expensive and cumbersome RF equipment like spectrum and network analyzers, to read the fragile signal out of the NEMS. The small signal strength, high resonance frequencies and large parasitic capacitances of the measurement setup generally do not allow for a direct read-out. This justifies the widespread mixer setup used to detect resonance [2]. Although mixing allows to detect resonance, it suffers from phase information loss, which limits the use of the NEMS sensor to open-loop configurations. With the goal of closing the loop, following frequency variations online and avoiding the use of rich RF lab equipment, we assess in this paper the potential of simple RF front-ends to sense and amplify the signal from the NEMS via a direct measurement in order to feed it back for sustained NEMS actuation. Design and validation via measurement of the feedback loop topology set the context for NEMS sensing in section II. The equivalent hybrid electromechanical interface is presented in section III, while section IV provides a prediction of the achievable noise figure and minimum detectable signal. Optimal front-end bias is the topic of section V and the predictions are validated via measurements of a 3-stage common emitter low-noise amplifier in section VI. Alternative front-end implementations are finally explored in section VII, before section VIII concludes on the potential of closed-loop emerging CNT-NEMS sensor applications.

All authors are with the Electronics Laboratory, Ecole Polytechnique Fédérale de Lausanne, CH-1015, Switzerland (see http://elab.epfl.ch).

II. Closed-loop CNT-NEMS Oscillator

The duty of the electronic feedback, a modified phase-locked loop (PLL) is to lock on the CNT's resonance frequency in order to steadily maintain the oscillation. The CNT can consequently be operated as a sensor and the information on sensed quantities is encoded in the frequency, extracted by the loop from the current flowing through the CNT. The exact working principle, illustrated by Fig.1, follows.

In the realm of electronics, carbon nanotubes have successfully been used in transistor configurations, operating the CNT as the channel material [3]. Defining the tube terminations as source and drain, in analogy to the MOS transistor, a nearby gate may control the current flow through the device. Clamping drain and source, while suspending the tube over a trench, adds mechanical degrees of freedom to the system. Driving the gate with a control voltage (a square wave in our implementation), induces an electrostatic force that sets the CNT into motion, with frequency f_0 at resonance.

This mechanical motion translates then back into an electrical signal via field- (with frequency f_0) and piezoresistive- (with frequency $2f_0$ due to oscillation symmetry) effects [4], which the front-end low-noise amplifier (LNA) [5] is to read and amplify in order to decode the motional information [6].

Given that parasitic coupling (with frequency f_0 at resonance) from the gate to the drain is inevitable and overshadows the field effect above 100MHz, bandpass filtering is necessary to isolate the piezoresistive component, carrying motional information. Detection of feeble signals of the NEMS substantially benefits from further reduced bandwidths, though the bandpass filter's quality factor must not exceed the NEMS'

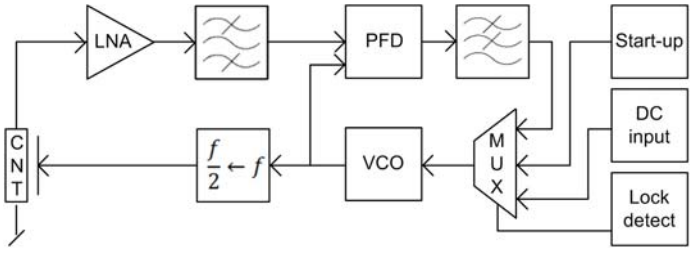

Fig. 1. Closed-loop topology for CNT-NEMS oscillator

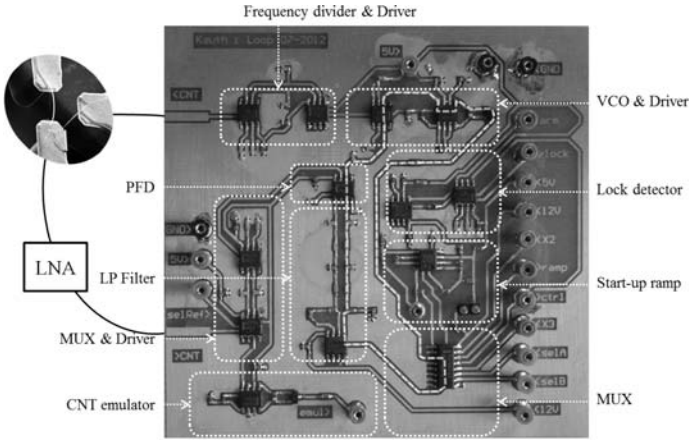

Fig. 2. PCB implementation of the feedback loop. PLL path appears dashed.

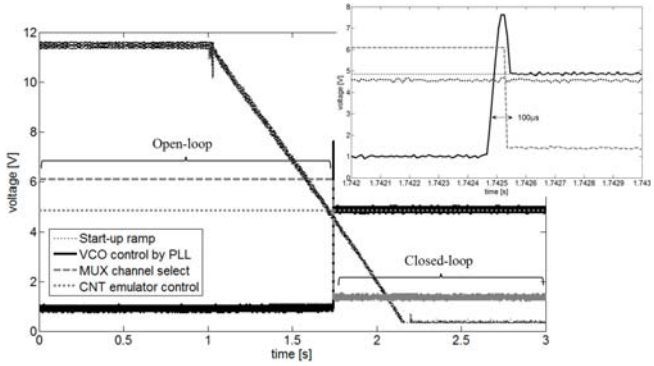

Fig. 3. Sweep and automatic lock detection measurement

one, which shall ultimately impose the locked loop frequency in sensor applications.

Near resonance, the phase-frequency detector (PFD) compares the phase and frequency of the NEMS's signal to the one of the voltage-controlled oscillator (VCO). The integral of the PFD's output is used to control this VCO and steadily adjust its frequency as to closely follow the signal received from the NEMS and stimulate it appropriately. Given that the piezoresistive component appears at twice the NEMS' mechanical motion, the frequency has to be halved before electrostatically actuating the NEMS for sustained oscillation.

Start-up of the CNT's mechanical motion requires an initial stimulus. This signal comes from the VCO, steered by a start-up sweep. Once the CNT is in motion and a signal has been detected by the LNA, a lock-detector block switches the multiplexer (MUX) and thus closes the loop, which consequently behaves as described above. A direct current (DC) input is foreseen for manual stimulation of the CNT, as a signal generator would do.

An implementation of the feedback loop has been realized on a printed circuit board (PBC), shown in Fig.2, and contains in addition to Fig.1 an on-board emulator of the CNT-NEMS, which allows for functional characterization of the loop at lack of a NEMS. The PLL can lock on signals ranging from 80MHz to 200MHz and is consequently able to stimulate and sustain resonance of CNTs with eigenfrequencies in the range from 40MHz to 100MHz, which covers the resonance spectrum of μm-long tubes with diverse diameters. The PCB has been tested successfully in the mentioned frequency range with the purely electronic on-board NEMS emulator.

The measured behaviour of the lock detection is provided in Fig.3. The MUX initially selects the start-up ramp, based on a Deboo integrator, to control the VCO and stimulate the NEMS with decreasing frequencies in an open-loop configuration. As long as this stimulus is above the CNT's resonance frequency f_0, the NEMS is not resonating and no signal is detected by the LNA, meaning that the low-pass filtered PFD signal is low and would require the VCO to slow down if the loop was closed. As soon as the ramp's voltage controls the VCO to the CNT's eigenfrequency (indicated by the horizontal line as an equivalent corresponding control voltage), the NEMS starts resonating, a signal is detected by the LNA and the PFD indicates that the falling start-up ramp is in the meanwhile generating a frequency below the NEMS' resonance, causing the low-pass filtered PDF output to bounce up, upon which the lock-detection circuit closes the loop by switching the MUX's channel selection. The closed-loop now locks within 100μs on the CNT's resonance frequency and tracks it, while the start-up ramp continues its decrease without any further effect on the loop's behaviour. The lock-in time-constant is primarily defined by the low-pass filter's time-constant and can be reduced if a more reactive lock-in is desirable. Note that the ratio of the ramp-down and lock-in time-constants must be chosen sufficiently large to ensure lock-in before the CNT leaves resonance again.

III. Hybrid Electromechanical Interface

The only remaining uncertainty that could protract the closed-loop's successful stimulation and tracking of a real NEMS' resonance is the strength and purity of the signal received from the CNT and the major concern for the rest of this paper is to design a low-noise front-end, providing the subsequent circuit stages with the best possible signal-to-noise ratio (SNR). The key to the best possible signal-to-noise ratio lies in the analysis of the hybrid electromechanical interface. As indicated in Fig.4, the CNT, biased to saturation, presents an output resistance, which comes with a noise current spectral density

$$S_{i^2,CNT} = \frac{4kT}{R_{CNT}} \tag{1}$$

and a parasitical source-drain capacitance, which circuit designers cannot impact. Follows in series a relatively large, noisy contact resistance $R_{contact}$, caused by mode reduction at the 3-dimensional metal to unidimensional CNT interface. For the following discussion, we suppose a decent NEMS design with a device that can be operated as a transistor and has measurable saturation, meaning that the contact resistance $R_{contact}$ is inferior to the CNT's output resistance R_{CNT}. This output resistance R_{CNT} is in the order of MΩ [7] and the parasitical capacitance C_{CNT} will typically not exceed hundreds of aF, guaranteeing an output impedance above MΩ up to GHz frequencies. Pads and wirebonding to take the signal from the chip out of the package onto the PCB, hosting the electronic front-end, will add in each case 1nH

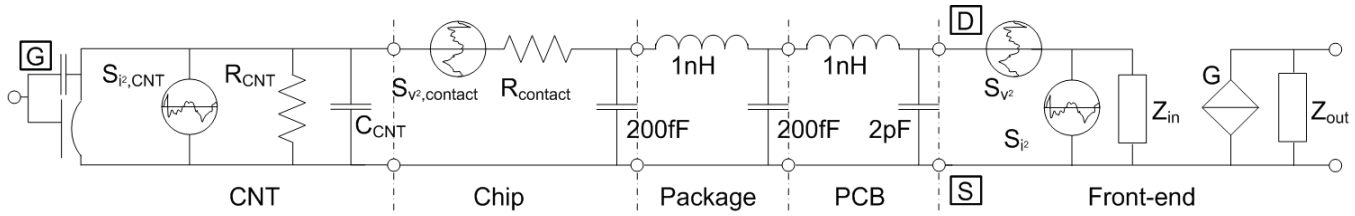

Fig. 4. Small signal equivalent circuit from NEMS to front-end

of inductance and a 200fF capacitance. On the PCB, the cumulative parasitical pad and track capacitance easily reaches C=2pF. Although this capacitance can be cancelled out via a parallel resonant circuit in narrow-band applications, we here target a wide-band front-end, that can adapt to the CNT's changing resonance frequency over a wide range upon sensing. With the aim of minimizing the front-end's noise figure (NF) and hence maximizing the system's overall SNR, we look next at an implementation of the generic front-end of Fig.4, namely the 3-stage common-emitter (CE) amplifier presented in Fig.5. Following a preliminary study of the noise-critical first stage in section IV, the full 3-stage amplifier is designed in section V and measured in VI.

IV. Noise Figure Prediction

Motivated by Friis' formula for the noise factor of a cascade of stages,

$$F_{total} = F_1 + \sum_{n=2}^{N} \frac{F_n - 1}{\prod_{i=1}^{n-1} G_i}, \tag{2}$$

where F_n is the noise factor of stage n and G_n the power gain of that same stage, we limit our analytical study to single-stage front-ends, loaded by a noisy resistance R_L. At sufficient gain, this first stage virtually defines the whole circuit's noise factor and its design merits special care. Though the system's noise figure is dominated by this first stage, a single-stage LNA may not provide sufficient gain or may simply not be optimal in terms of noise figure if compelled to transform the nA current out of the CNT into some tens of mV necessary to properly stimulate the PFD down the loop.

The real design challenge formulates as a constrained optimization problem, having as objective a minimal LNA noise figure, constrained by sufficient signal amplification, stable gain and transistor bias limitations. This problem has been solved via Sequential Quadratic Programming for given devices and proved 3-stage topologies to be nearly optimal in the MHz to GHz range if bipolar junction transistors (BJT) are used in common-emitter (CE) configuration. Such a 3-stage CE LNA will be designed and characterized in sections V & VI. As a matter of fact, all but 1dB of the noise figure comes from the most noise critical first stage, which allows us to reduce the following noise analysis to a single-stage LNA operating a BJT in common emitter configuration. Its small signal schematic, including all white noise sources, is shown by the inset of Fig.6. CNT-NEMS operating generally in the MHz to GHz frequency range, hypothesizing operation above the device 1/f-corner frequency [8] is reasonable and one may thus safely neglect Flicker noise. The circuit's noise contributions come from the BJT's shot noise at base and collector, completed by the load's thermal noise. Connecting this front-end to the CNT as suggested in Fig.4, leads to the following noise factor expression

$$\begin{aligned} F_{CE} = & \quad 1 & \text{by CNT} \\ & + \frac{\gamma}{\beta^2} R_{CNT} G_m \left[1 + \left(\omega \frac{\beta C}{G_m}\right)^2\right] & \text{by collector} \\ & + \frac{\gamma}{\beta} R_{CNT} G_m & \text{by base} \\ & + \frac{R_{CNT}}{\beta^2 R_L} \left[1 + \left(\omega \frac{\beta C}{G_m}\right)^2\right] & \text{by load,} \end{aligned} \tag{3}$$

where G_m is the transconductance, γ the noise excess factor, β the current gain, and C is the parasitic interconnect capacitance, overshadowing any base-emitter coupling. The noise figure

$$NF = 10 \log F, \tag{4}$$

is plotted against frequency on Fig.6, indicating the existence of an optimal bias-point according to the targeted operation frequency. The important NF values result from the com-

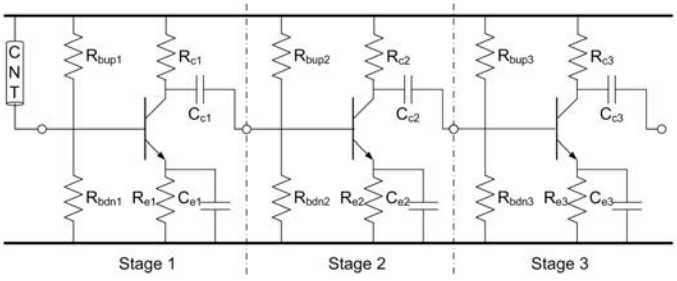

Fig. 5. 3-stage biased CE low-noise amplifier

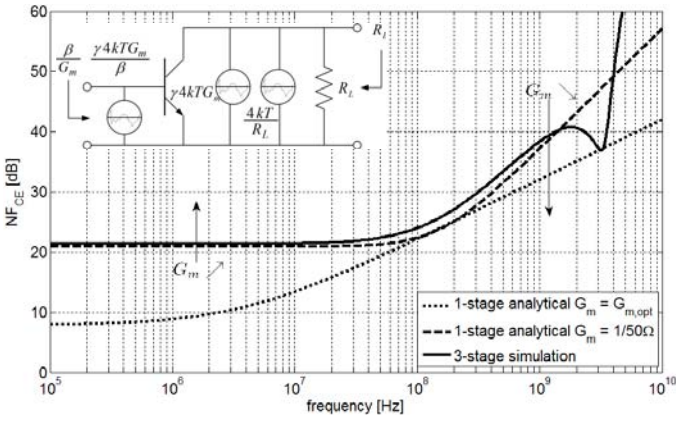

Fig. 6. NF of CE front-end with C=2pF, R_{CNT}=1MΩ, R_L=1kΩ

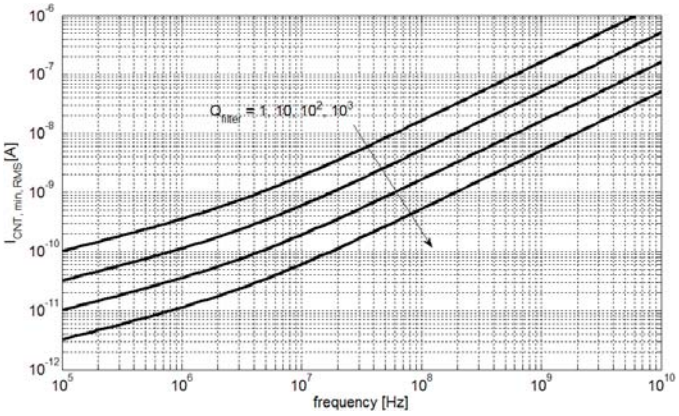

Fig. 7. Minimal detectable current from CNT with R_{CNT}=1MΩ through 2pF interconnects with a CE (β=100) front-end at ambient temperature for SNR$_{out}$=1.

bination of the CNT's large output impedance and the pF interconnect capacitance. Given that CE topologies possess enough power gain to subvert the load's noise contribution, the NF is limited by the base noise at low frequencies and by the collector noise at high frequencies. The continuous line corresponds to the simulated NF of the 3-stage CE front-end, designed to operate at 100MHz and presented subsequently. One can observe that the 3-stage simulation follows rather well the 1-stage analytical prediction, portending that the noise contribution of stages 2 and 3 remains negligible with respect to the first stage's noise.

V. System Bias

The 3-stage CE front-end henceforth considered is depicted in Fig.5. Insensitive to the transistors' current gain β, the bias networks of each stage are decoupled via capacitors C_{ci}. The base potential is a free design variable and hence presents a degree of freedom that, in the case of the first stage, can be exploited to adjust the base voltage as to properly set the CNT's DC bias to roughly 1 to 10 μA [9] (voltage-bias). The emitter capacitance C_{ei} grounds the bias resistor R_{ei} over the widest feasible bandwidth to avoid noise contributions and negative feedback. Choosing R_{up1} and R_{dn1} larger than the BJT's input impedance $\frac{\beta}{G_m}$, renders their contribution to the noise figure insignificant. To keep the biasing independent from the current gain β, current through the base biasing resistors shall render the BJT base current negligible. The last two constraints can be achieved simultaneously by providing sufficient voltage supply. The optimal stage-1 collector current follows from derivation of expression (3) with respect to G_m, yielding

$$I_{C0,opt} = \sqrt{2\beta}\frac{kT}{q}\omega C, \tag{5}$$

with q the elementary positive charge. The bias of the subsequent stages may be chosen as to provide maximum stable gain, as their impact on the NF is less significant. For such an optimal bias, the minimal detectable current variation out of the CNT is given by

$$I_{CNT,RMS} \geq \sqrt{\frac{4kTB}{R_{CNT}} \cdot F_{opt} \cdot \text{SNR}_{out}}, \tag{6}$$

where B is the bandwidth of the subsequent filter and SNR$_{out}$ the desired signal to noise ratio at the output of the filter. Fig.7 suggests that the optimally biased CE front-end is reliant on the use of filters to detect CNT currents of nA amplitude at resonance frequencies above tens of MHz.

VI. Measurements

With the objective of validating the previous conclusions drawn for the CE front-end interfacing a CNT-NEMS, exclusively based on analytical analyses and simulations, this section confronts the simulations with measurement results for the 3-stage CE front-end in the common 50Ω RF framework. Although the absolute values of gain and NF happen to be very different from what they would be in the CNT MΩ framework, the mere fact that the measurements match the simulation (see Fig.9 & 10), provides the necessary provisional faith into the previously drawn conclusions on noise figure (see Fig.6) and minimal detectable signal from the CNT-NEMS (see Fig.7). A next step consists in verifying those predictions via measurement on a real CNT-NEMS.

The PCB in question is depicted on Fig.8. 50Ω impedance matching was omitted, as the front-end is primarily meant for MΩ NEMS interfaces. The measured and simulated forward power gain is plotted on Fig.9. The low-pass cut-off is due to the pole defined by $\omega_{p1} = \frac{G_m}{C_e}$. Although it is possible to extend the passband to lower frequencies, a second high-pass pole limits this endeavour at $\omega_{p2} = \frac{1}{(R_{in}+R_c)C_c}$, R_{in} being the input impedance of the next stage, speak $\frac{\beta}{G_m}$. While the measured pass-band frequencies were accurately predicted by the simulation, its gain presents an 8dB discrepancy. The power gain in the passband writing

$$|S_{21}|^2 = 20\log\frac{2\beta G_m R_c}{\beta + G_m R_c}, \tag{7}$$

the difference between measured and simulated current gains β accounts for twice 1.9dB and the cabling losses for 0.4dB, leaving 3.8dB of yet unexplained discrepancy. More importantly does the NF, shown in Fig.10, confirm that the simulation predicts the measurement trend up to the front-end's gain

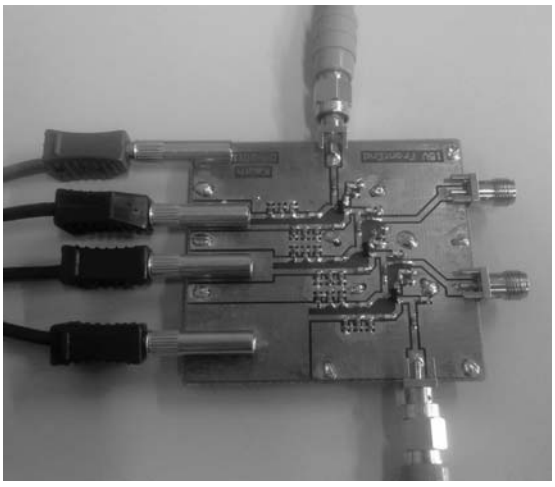

Fig. 8. 3-stage discrete component CE front-end

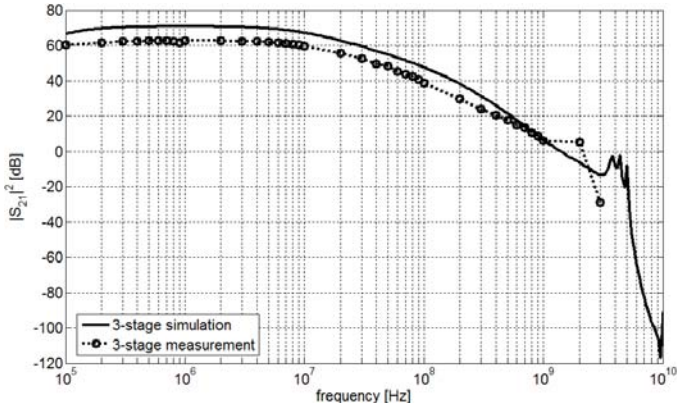

Fig. 9. 3-stage CE forward power gain in 50Ω framework

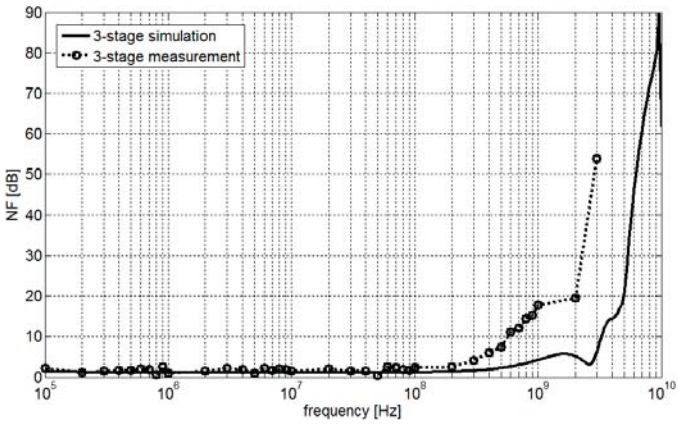

Fig. 10. 3-stage CE noise figure in 50Ω framework

decay. By this validation principle, we can prognosticate for the CE front-end a NF similar to the simulated one of Fig.6 when interfacing the CNT-NEMS, implying an upper bound on signal sensitivity provided by Fig.7.

VII. Alternative Topologies

To conclude this round-trip on RF front-ends for CNT-NEMS sensors, we briefly highlight 3 alternate topologies:

A. Common base

The common base (CB) front-end, represented in the inset of Fig.11, also relies on bipolar technology. Compared to the CE, it presents a larger pass-band at the cost of a unity current gain. This implies a stronger noise contribution from the load, as emanates from

$$\begin{aligned} F_{CB} = & \quad 1 & \text{by CNT} \\ & + \quad \tfrac{\gamma}{\beta^2} R_{CNT} G_m \left[1 + \left(\omega \tfrac{\beta C}{G_m}\right)^2\right] & \text{by collector} \\ & + \quad \tfrac{\gamma}{\beta} R_{CNT} G_m & \text{by base} \\ & + \quad \tfrac{R_{CNT}}{R_L} \left[1 + \left(\omega \tfrac{C}{G_m}\right)^2\right] & \text{by load.} \end{aligned} \tag{8}$$

At low frequencies, the NF is limited by load and base shot noise, while the collector shot noise dominates at high frequencies. Although a large load enhances gain and noise performance at low frequencies, the performance of a CB front-end remains inferior to the CE in terms of noise and gain.

B. Common source

The noise of metal-oxide-semiconductor (MOS) front-ends can be summarized to the channel thermal noise, with negligible gate-induced noise in the considered frequency range. Its immense input impedance makes the common source (CS) an ideal candidate for low NF at relatively low frequencies, as arises from Fig.12. The NF, given by

$$\begin{aligned} F_{CS} = & \quad 1 & \text{by CNT} \\ & + \quad \tfrac{\gamma}{R_{CNT} G_m} \left[1 + (\omega R_{CNT} C)^2\right] & \text{by channel} \\ & + \quad \tfrac{1}{G_m^2 R_{CNT} R_L} \left[1 + (\omega R_{CNT} C)^2\right] & \text{by load,} \end{aligned} \tag{9}$$

can be enhanced at any frequency at the cost of a larger biasing current. At low frequencies, the SNR is limited by the CNT noise, while the channel noise is responsible for the increasing NF at high frequencies. On the downside, a CS interface requires a more sophisticated current-bias of the NEMS.

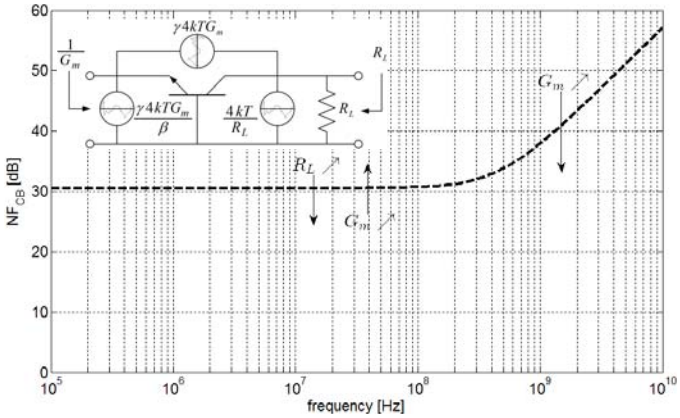

Fig. 11. NF of CB front-end with C=2pF, R_{CNT}=1MΩ, R_L=1kΩ, $1/G_m$=50Ω

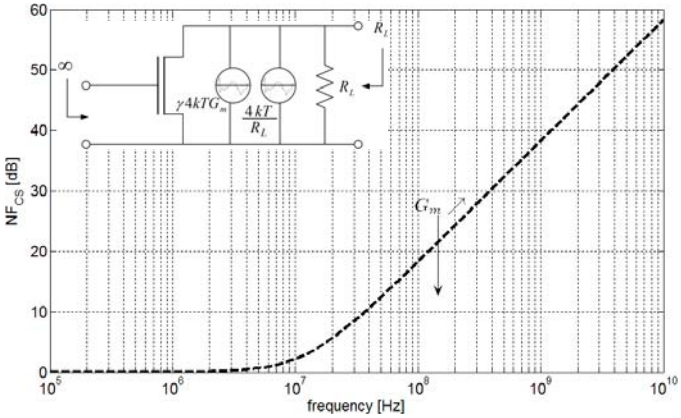

Fig. 12. NF of CS front-end with C=2pF, R_{CNT}=1MΩ, R_L=1kΩ, $1/G_m$=50Ω

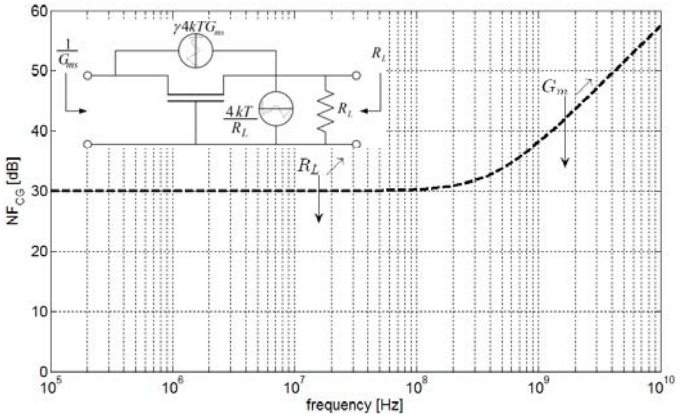

Fig. 13. NF of CG front-end with C=2pF, R_{CNT}=1MΩ, R_L=1kΩ, $1/G_{ms}$=50Ω

C. Common gate

Large load and voltage gain are beneficial to a common gate (CG) topology at low frequencies. As for the CS front-end, at high frequencies, increased bias current enhances the NF

$$\begin{aligned} F_{CG} = & \quad 1 & \text{by CNT} \quad (10)\\ & + \quad \frac{\gamma}{R_{CNT}G_{ms}}\left[1+(\omega R_{CNT}C)^2\right] & \text{by channel}\\ & + \quad \frac{R_{CNT}}{R_L}\left[1+\left(\omega\frac{C}{G_{ms}}\right)^2\right] & \text{by load.} \end{aligned}$$

Its noise performance is comparable to the one of CB and suffers from stronger noise contribution from the load, compared to the CS topology.

D. Common collector & Common drain

Common collector (CC) and common drain (CD) are inherently high impedance topologies, which require more complex current-biasing of the NEMS. In terms of noise figure and gain, none of these topologies is preferable to CE and CS respectively. While the CD noise figure is identical to the CS one, CC suffers from increased base shot noise contribution to the noise figure with respect to CE topologies, due to its higher input impedance.

VIII. Conclusion

A closed-loop circuit for carbon-nanotube NEMS oscillators has been presented. Start-up and lock detection circuitry allow for NEMS actuation, resonance lock and maintenance upon drift in sensing applications. The printed circuit board implementation of the modified phase-locked loop grounds on the piezoresistive property of carbon nanotubes and is designed for CNT resonators from 40MHz to 100MHz, covering a wide tube diameter and length distribution for roughly μm-long tubes.

Different topologies of the utterly noise-critical LNA block have been considered and a 3-stage common emitter front-end was designed, analyzed and characterized. It was found to present large noise figures in the MHz to GHz frequency range, when interfacing a carbon-nanotube NEMS. This significant noise contribution of the circuit is inherently ascribed to the NEMS' high output impedance in combination with a pico-farad interconnect capacitance.

The minimal detectable signal out of a CNT-NEMS resonating at 100MHz was evidenced to be in the order of tens of nano-amps for a wide-band common emitter front-end, optimally biased for minimum noise. This limit can be bypassed in narrow-band applications either by resonating out the interconnection parasitical capacitance with a parallel LC circuit or by using a subsequent band-pass filter stage.

Finally the common source front-end was shown to be a promising candidate for low frequency sensing (up to tens of MHz), due to its insignificant contribution to the system's signal-to-noise ratio in this frequency range, subject to NEMS current-biasing.

Acknowledgment

This research has been funded by Nano-Tera.ch, a program of the Swiss Confederation, evaluated by SNSF.

References

[1] H. B. Peng, C. W. Chang, S. Aloni, T. D. Yuzvinsky, and A. Zettl, "Ultrahigh frequency nanotube resonators," *Phys. Rev. Lett.*, vol. 97, no. 8, p. 087203, Aug 2006.

[2] V. Sazonova, Y. Yaish, H. Ustunel, D. Roundy, T. A. Arias, and P. L. McEuen, "A tunable carbon nanotube electromechanical oscillator," *Nature*, vol. 431, no. 7006, pp. 284–287, Sep. 2004.

[3] J. Chaste, L. Lechner, P. Morfin, G. Feve, T. Kontos, J. Berroir, D. Glattli, H. Happy, P. Hakonen, and B. Placais, "Single carbon nanotube transistor at ghz frequency," *Nano Letters*, vol. 8, no. 2, pp. 525–528, 2008.

[4] M. Huang, Y. Wu, B. Chandra, H. Yan, Y. Shan, T. F. Heinz, and J. Hone, "Direct measurement of strain-induced changes in the band structure of carbon nanotubes," *Phys. Rev. Lett.*, vol. 100, p. 136803, Apr 2008.

[5] C. Kauth, M. Pastre, and M. Kayal, "Wideband low-noise rf front-end for cnt-nems sensors," *Mixed Design of Integrated Circuits and Systems conference proceedings*, pp. 289–293, May 2012.

[6] G. Y. Guo, L. Liu, K. C. Chu, C. S. Jayanthi, and S. Y. Wu, "Electromechanical responses of single-walled carbon nanotubes: Interplay between the strain-induced energy-gap opening and the pinning of the fermi level," vol. 98, no. 4, p. 044311, 2005.

[7] *Carbon Nanotubes: Properties and Applications*. CRC, 2006, p. 93.

[8] P. G. Collins, M. S. Fuhrer, and A. Zettl, "1/f noise in carbon nanotubes," *Applied Physics Letters*, vol. 76, no. 7, pp. 894–896, 2000.

[9] A. Javey, J. Guo, D. Farmer, Q. Wang, E. Yenilmez, R. Gordon, M. Lundstrom, and H. Dai, "Self-aligned ballistic molecular transistors and electrically parallel nanotube arrays," *Nano Letters*, vol. 4, no. 7, pp. 1319–1322, 2004.

Christian Kauth received the B.S. in electrical engineering and M.S. in micro- and nanotechnologies for integrated systems from EPFL in 2007 and 2009 respectively. He works towards the Ph.D. degree at EPFL with research interests in carbon nanotube physics, MEMS oscillator design and algorithms.

Marc Pastre received the B.S. and M.S. degrees in computer science and the Ph.D. degree in microelectronics from EPFL in 2000 and 2005 respectively. His research interests include low-power analog and mixed-signal circuits, ADCs/DACs, high-performance sensor interfaces, digital enhancement of analog circuits and CAD tools.

Maher Kayal received the M.S. and Ph.D degrees in electrical engineering from EPFL in 1983 and 1989 respectively. He is currently a professor and vice dean for education of the school of engineering at EPFL. Author of many scientific papers, coauthor of three text books on mixed-mode CMOS design and holder of seven patents, his technical contributions have been in analog and mixed-signal circuits design including highly linear and tunable sensor microsystems, signal processing and CAD tools for analog design and layout automation. He received the Swiss Ascom award in 1990 for the best work in telecommunications and the Swiss Credit best teaching award in 2009.